Small-Signal Synchronization Stability Enhancement of Grid-Following Inverters via a Feedback Linearization Controller

Milad Zarif Mansour, *Graduate Student Member, IEEE,* Mohammad Hasan Ravanji, *Member, IEEE,* Alireza Karimi, *Senior Member, IEEE,* Behrooz Bahrani, *Senior Member, IEEE*

***Abstract*—This paper proposes a feedback linearization controller for a grid-following inverter (GFLI) that uses a conventional Phase-Locked Loop (PLL) as the synchronization unit. The proposed controller enhances the GFLI synchronization by expanding the PLL domain of attraction to the whole plane that is limited to a small region around the equilibrium point in a conventional PLL, provided that the grid impedance and voltage are known. Linearizing the overall closed-loop system, the proposed controller provides linear system attributes for the PLL, leading to an infinite domain of attraction and only one equilibrium point. Additionally, a state-feedback controller is integrated within the feedback linearization controller so that it enables the system to have an adjustable dynamic response. Finally, it is shown that the system is robust against parametric uncertainties. The performance of the proposed control design is validated in Matlab/Simulink and experiment. It is verified that the proposed controller expands the domain of attraction and enhances the system dynamic response.**

***Index Terms*—Domain of Attraction, Feedback Linearization, Phase-Locked Loop, State Feedback, Vector Current Control.**

I. Introduction

INVERTER-BASED resources (IBRs) are increasingly becoming an inseparable part of the energy industry in light of their declining cost and lower carbon dioxide emission. As a result, their deployment in various power systems is swiftly increasing, and they are displacing the conventional synchronous generators. IBRs connected to weak grids, however, may encounter stability and synchronization issues as a result of conventional control structures and synchronization techniques deficiencies [1], [2]. Based on the employed synchronization method, IBRs can be categorized as 1) grid-following inverters (GFLIs) and 2) grid-forming inverters (GFMIs). GFLIs use a Phase-Locked Loop (PLL) for extracting the grid voltage angle and getting synchronized to the grid [3]–[5]. To this end, the point of connection (PoC) voltage is used by the PLL, and the grid voltage frequency and angle are estimated, which are used in the current control loop [6]–[8]. Contrary to the GFLIs, GFMIs do not use a PLL for synchronization [9]. Rather, the inverter active power is controlled by adjusting the PoC voltage angle [10]. This study focuses on the synchronization issues present in GFLIs.

In the existing literature, GFLIs stability analysis is classified into two main categories: 1) small-signal and 2) large-signal synchronization stability [10]. Small-signal synchronization stability analysis studies the stability issues due to small disturbances by system linearization around the operating point and the use of linear control approaches [11]. For this purpose, eigenvalue-based and impedance-based analyses are two well-known approaches [12], [13]. On the other hand, large-signal synchronization stability analysis investigates the impact of large disturbances on the stability. It is shown that large-signal stability is threatened by the loss of synchronization, occurring due to the PLL failure [14]. In this type of stability analysis, as a result of the system nonlinear nature, initially, the presence of an equilibrium point during the disturbance must be studied, and the convergence of the states to this point must be assessed [15]–[19]. This paper, however, focuses on the small-signal synchronization stability of GFLIs.

The previous studies on the small-signal synchronization stability try to propose mitigation techniques for the PLL. For instance, a bandwidth reduction method is proposed in [20], and a damping controller is proposed by [21]. Also, virtual impedance-based methods for mitigating the small-signal synchronization stability are widely studied in previous studies [21]–[23]. Besides, the majority of the previous studies on the large-signal stability enhancement focus on the fault rid-through (FRT) schemes. In this regard, some studies propose active and reactive current alteration [24], [25]. Ref. [26] proposes an adaptive current injection technique that changes the current references upon fault occurrence to prevent IBR instability. This method requires accurate information of the grid impedance and a fault detection scheme. Some other studies target the main source of large-signal instability, i.e., the PLL. Freezing the PLL during a fault is proposed in [27], [28]. Some other studies propose increasing PLL damping factor by increasing and decreasing the PLL PI controller proportional and integral gains, respectively [24], [29]. Also, a gain-scheduled integral gain method is proposed in [30]. Some other studies propose modifying the PLL to a first-order loop during the fault by removing the integrator within the PI controller [31], [32].

Most of the previous studies on small-signal synchronization stability neglect the system nonlinearity and equilibrium point domain of attraction. Additionally, the studies investigating the large-signal stability enhancement mainly focus on presenting FRT schemes to keep the PLL stable in the presence of fault occurrences. In other words, these approaches do not help the PLL to remain stable during the normal operation, and the PLL must be meticulously designed while the IBR is integrated into weak grids [10]. Moreover, due to the changes in the IBR operating point and the grid, the initially designed PLL may not be able to maintain stability and have a proper domain of attraction. To address the aforementioned shortcomings, this paper proposes a feedback linearization compensator for the

PLL that eliminates the system nonlinearity and expands the system domain of attraction to the whole plane provided that the grid impedance and voltage are known. It should be noted that this article does not propose an FRT scheme, and hence, it does not study the system in the presence of faults. Additionally, to have the flexibility for the PLL response, a state-feedback outer controller is added to the proposed compensator as well. The benefit of the proposed controller is that it does not depend on the initially designed PLL, i.e., in case the initial PLL is not optimal for any reason, e.g., operating point changes, the proposed controller forces the closed-loop system to have the desired dynamic response. The proposed controller:

- expands the domain of attraction as a result of linearizing the system,
- stabilizes the system regardless of the initially designed PLL,
- forces the PLL to have the desired performance regardless of the operating point, short circuit ratio (SCR), and the PLL initial design.

Moreover, this study provides a robustness analysis for the proposed controller with respect to the grid impedance and grid voltage estimation errors. It is mathematically shown that the proposed controller remains stable in the presence of a considerable grid inductance or voltage estimation errors. Also, simulation results are provided to compare the conventional and compensated PLLs in the presence of grid faults. Although this study does not theoretically evaluate the system stability during the fault, it is seen from the simulation results that the compensated PLL outperforms the conventional one in the presence of a grid fault.

The rest of this paper is organized as follows. Section II introduces the nonlinear model of the PLL. Section III describes the proposed feedback linearization and state-feedback control design, and carries out the closed-loop robustness analysis. The performance of the proposed method is assessed via simulation and experiment in Section IV. Finally, the conclusions are presented in Section V.

II. Nonlinear Model of a Grid-connected Inverter

The block diagram of a GFLI and its corresponding control loops are shown in Fig. 1. In this study, a Synchronous Reference Frame PLL (SRF-PLL) is chosen as the GFLI synchronization unit whose structure is shown in Fig. 2. Suppose that the proportional and integral gains used in the PLL PI controller are K_p and K_i, respectively. Additionally, assume v_{q} is the PoC voltage q-component, ω_0 is the grid nominal frequency, and θ is the PLL estimated angle. By neglecting the current controller dynamics (since it is designed much faster than the PLL), the integral equation describing the PLL dynamics can be written as [15]

$$\theta = \int \left[\left(K_p v_{\mathrm{q}} + \int K_i v_{\mathrm{q}} \mathrm{d}t \right) + \omega_0 \right] \mathrm{d}t, \tag{1}$$

where

$$v_{\mathrm{q}} = V_{\mathrm{g}} \sin(-\delta) + |Z_L(\omega)| I_{\mathrm{PoC}} \sin(\theta_I + \phi_c(\omega)) \tag{2}$$

and

$$\phi_c(\omega) = \measuredangle Z_L(\omega). \tag{3}$$

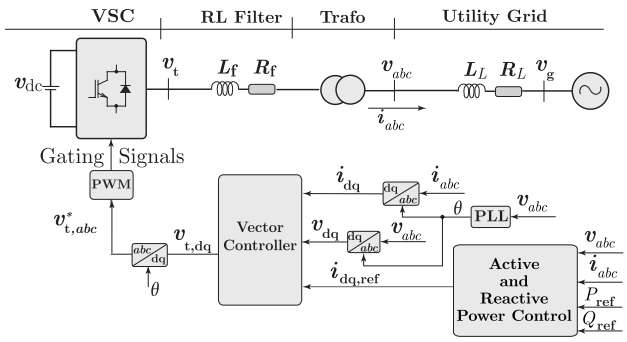

Fig. 1. The block diagram of a GFLI and the corresponding control blocks.

In (2) and (3), V_{g} is the magnitude of the grid phase voltage vector, $Z_L(\omega)$ and $\phi_c(\omega)$ are the grid impedance and its angle, I_{PoC} and θ_I are the IBR injected current vector magnitude and its angle with respect to the PoC voltage, the angle difference between the grid and PoC voltages is δ, and ω is the PLL estimated frequency.

By differentiating (1) twice with respect to time, the differential equation describing the PLL dynamics can be written as

$$\begin{aligned} \ddot{\delta} = K_p \left(-\dot{\delta} V_{\mathrm{g}} \cos\delta + \frac{\mathrm{d}(|Z_L| I_{\mathrm{PoC}} \sin(\theta_I + \phi_c(\omega)))}{\mathrm{d}t} \right) \\ + K_i (|Z_L| I_{\mathrm{PoC}} \sin(\theta_I + \phi_c(\omega)) - V_{\mathrm{g}} \sin\delta), \end{aligned} \tag{4}$$

which can be re-written as

$$\begin{aligned} \ddot{\delta} = K_p \left(-\dot{\delta} V_{\mathrm{g}} \cos\delta + \frac{\mathrm{d}(R_L I_{\mathrm{PoC}} \sin\theta_I + L_L \omega I_{\mathrm{PoC}} \cos\theta_I)}{\mathrm{d}t} \right) \\ + K_i (|Z_L| I_{\mathrm{PoC}} \sin(\theta_I + \phi_c(\omega)) - V_{\mathrm{g}} \sin\delta), \end{aligned} \tag{5}$$

given $|Z_L(\omega)| \sin\phi_c = L_L\omega$ and $|Z_L(\omega)| \cos\phi_c = R_L$. By expanding (5) and considering that $\omega = \omega_0 + \dot{\delta}$, the differential equation can be re-arranged as

$$\begin{aligned} \ddot{\delta} = -K_p V_{\mathrm{g}} \dot{\delta} \cos\delta + K_p L_L I_{\mathrm{PoC}} \ddot{\delta} \cos\theta_I + K_i R_L I_{\mathrm{PoC}} \sin\theta_I \\ + K_i L_L \omega_0 I_{\mathrm{PoC}} \cos\theta_I + K_i L_L I_{\mathrm{PoC}} \dot{\delta} \cos\theta_I - K_i V_{\mathrm{g}} \sin\delta, \end{aligned} \tag{6}$$

where $\dot{\delta}$ and $\ddot{\delta}$ are the first and second derivatives of δ with respect to time, respectively. Using (6) and defining $\hat{x}_1 = \delta$ and $\hat{x}_2 = \dot{\delta}$, the state-space model of the system can be written as

$$\begin{cases} \dot{\hat{x}}_1 = \hat{x}_2, \\ \dot{\hat{x}}_2 = B - D \sin\hat{x}_1 + (A \cos\hat{x}_1 + C)\hat{x}_2, \end{cases} \tag{7}$$

where A, B, C and D are

$$\begin{aligned} A &= \frac{-K_p V_{\mathrm{g}}}{1 - K_p L_L I_{\mathrm{PoC}} \cos\theta_I}, \\ B &= \frac{K_i R_L I_{\mathrm{PoC}} \sin\theta_I + K_i L_L \omega_0 I_{\mathrm{PoC}} \cos\theta_I}{1 - K_p L_L I_{\mathrm{PoC}} \cos\theta_I}, \\ C &= \frac{K_i L_L I_{\mathrm{PoC}} \cos\theta_I}{1 - K_p L_L I_{\mathrm{PoC}} \cos\theta_I}, \\ D &= \frac{K_i V_{\mathrm{g}}}{1 - K_p L_L I_{\mathrm{PoC}} \cos\theta_I}. \end{aligned} \tag{8}$$

In (7), the equilibrium point of the system is $(\hat{x}_1^e, \hat{x}_2^e) = (\sin^{-1}(\frac{B}{D}), 0)$. Assuming $\hat{x}_1 = x_1 + \alpha$, where $\alpha = \sin^{-1}(\frac{B}{D})$, and $\hat{x}_2 = x_2$, the equilibrium point of the

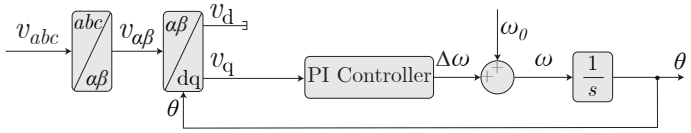

Fig. 2. The block diagram of an SRF-PLL.

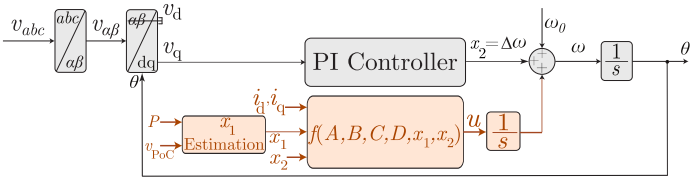

Fig. 3. The block diagram of a compensated SRF-PLL.

system can be transferred to the origin, and the state-space equations can be re-written as

$$\begin{cases} \dot{x}_1 = x_2 = f_1(x_1, x_2), \\ \dot{x}_2 = B - D\sin(x_1+\alpha) + (A\cos(x_1+\alpha)+C)x_2 \\ \quad = f_2(x_1, x_2) \end{cases}. \tag{9}$$

As shown in [19], the domain of attraction of the equilibrium point is a limited area around the origin, meaning that large disturbances can cause instability in the system. Additionally, IBRs connected to weaker systems have smaller domains of attraction, making them prone to instability due to minor disturbances. Moreover, if the grid becomes very weak, i.e., the grid impedance increases drastically, the equilibrium point becomes unstable.

This paper proposes a feedback linearization compensator for the PLL that can stabilize the system while connected to very weak grids and expand the domain of attraction to the whole plane. As a result, large disturbances cannot cause instability in the system, and the stability can be enhanced significantly.

III. Feedback Linearization Control Design for a GFLI

In the previous section, the nonlinear state-space model describing the PLL is derived. In this section, using a feedback-linearization controller, the domain of attraction is extended to the whole plane, and the nonlinear system is completely linearized.

Suppose that a control law, u, is added to the second state-equation in (9), changing the state-space model to

$$\begin{cases} \dot{x}_1 = x_2, \\ \dot{x}_2 = B - D\sin(x_1+\alpha) + (A\cos(x_1+\alpha)+C)x_2 + u \end{cases}. \tag{10}$$

To satisfy the infinite domain of attraction goal, the control law should be chosen such that the nonlinearities in the system dynamics are eliminated. Also, adding two linear terms consisting of both states adds two degrees of freedom for obtaining the desired closed-loop performance to u. Hence, the control law can be chosen as

$$\begin{aligned} u = &- B + D\sin(x_1+\alpha) - (A\cos(x_1+\alpha)+C)x_2 \\ &- k_1x_1 - k_2x_2, \end{aligned} \tag{11}$$

By replacing the feedback linearization control law shown in (11) in (10), the state-space equations of the compensated system can be written as

$$\begin{cases} \dot{x}_1 = x_2, \\ \dot{x}_2 = -k_1x_1 - k_2x_2 \end{cases}, \tag{12}$$

which is a stable, linear system. Additionally, the domain of attraction of the equilibrium point in a linear system is the whole plane, satisfying this study initial purpose. This is valid even after a severe disturbance clearance, such as fault clearances, since the grid voltage and impedance that may alter during the disturbance return to their nominal values. Also, the controller uses the measured injected current, resulting in a complete linearization, and hence, making the system domain of attraction the whole plane. However, this requires the system states do not diverge to infinity prior to the disturbance clearance. To have the desired response, k_1 and k_2 can be adjusted accordingly.

It is worth mentioning that the above-mentioned equations are all written in a per-unit system, and if the PLL is not implemented in a per-unit system, the state-equations used for the state-feedback controller design are slightly changed by setting $\frac{1}{\omega_0}\dot{x}_1{=}y_2$, in which x_1 and y_2 are physical states. Hence, the state-equations can be written as

$$\begin{cases} \dot{x}_1 = \omega_0 y_2, \\ \dot{y}_2 = -k_1x_1 - k_2y_2 \end{cases}, \tag{13}$$

and supposing the angular frequency is the output, the corresponding transfer function can be written as

$$g(s) = \frac{\omega_0}{s^2 + k_2 s + k_1\omega_0}. \tag{14}$$

Based on the transfer function shown in (14), the system damping ratio is $\zeta{=}\frac{k}{2\sqrt{k_1\omega_0}}$, and the natural angular frequency is $\omega_n{=}\sqrt{k_1\omega_0}$. Using these equations, the system rise time and overshoot can be set by adjusting k_1 and k_2.

A. Feedback Linearization Implementation

As shown in (10), the feedback linearization control law is added to $\dot{x}_2$, which is not physically available based on the PLL block diagram unless the proportional term within the employed PI controller is set to zero, i.e., an integrator is used as the controller instead of a PI controller. Therefore, instead of adding the control law to $\dot{x}_2$, its integral is added to x_2, i.e., the PI controller output. The block diagram of the compensated PLL is shown in Fig. 3. In this figure, the states and the injected i_{dq} are measured and used for forming the control law. Afterwards, the control law is integrated and added to x_2, i.e., the PI controller output.

B. Robustness Analysis

The feedback linearization and state-feedback controllers are proposed assuming that the grid impedance and voltage magnitude are known and constant. It is a fair assumption that the grid voltage magnitude is known and equal to the grid nominal voltage in the transmission level, except during a fault

occurrence. Additionally, there are effective and accurate online and offline methods for grid impedance estimation [33], [34]. However, in this part, the impact of errors in the grid inductance estimation and voltage on the compensated system stability is analyzed. It should be noted that in this part, Lyapunov's first theorem is employed to find the necessary and sufficient conditions for the equilibrium point stability. Additionally, since in the presence of estimation errors, the proposed controller cannot linearize the system utterly, the domain of attraction is not the whole plane anymore. Hence, a Lyapunov energy function should be employed to find the domain of attraction. This article proposes a Lyapunov function for when grid voltage estimation error is present in the controller, which can be used for finding the domain of attraction. A similar approach can be used for finding the domain of attraction when the grid impedance estimation is not accurate.

1) Grid Voltage Estimation Error: In case an accurate estimation of the grid voltage is not available, A and D coefficients of the system shown in (8) will be different from what is used in forming $\tilde{u}$. Supposing that the new coefficients are $\tilde{A}$ and $\tilde{D}$, the state-equations of the compensated system can be written as

$$\begin{cases} \dot{x}_1 = x_2, \\ \dot{x}_2 = -\tilde{D}\sin(x_1+\tilde{\alpha}) + D\sin(x_1+\alpha) + \tilde{A}\cos(x_1+\tilde{\alpha})x_2 \\ \quad -A\cos(x_1+\alpha)x_2 - k_1x_1 - k_2x_2 \end{cases}, \tag{15}$$

in which $\tilde{\alpha} = \arcsin(\frac{B}{\tilde{D}})$. By linearizing the system around the equilibrium point, i.e., the origin, the Jacobian matrix can be found as

$$J = \begin{pmatrix} 0 & 1 \\ -\sqrt{\tilde{D}^2 - B^2} + \sqrt{D^2 - B^2} - k_1 & \tilde{A}\cos(\tilde{\alpha}) - A\cos(\alpha) - k_2 \end{pmatrix}. \tag{16}$$

By naming

$$e_1 = -\sqrt{\tilde{D}^2 - B^2} + \sqrt{D^2 - B^2}, \tag{17}$$

and

$$e_2 = \tilde{A}\cos(\tilde{\alpha}) - A\cos(\alpha) = \frac{A}{D}(\sqrt{\tilde{D}^2 - B^2} - \sqrt{D^2 - B^2}), \tag{18}$$

the Jacobian matrix becomes

$$J = \begin{pmatrix} 0 & 1 \\ e_1 - k_1 & e_2 - k_2 \end{pmatrix}, \tag{19}$$

and hence, the stability condition becomes $k_1 > e_1$ and $k_2 > e_2$.

To evaluate the system domain of attraction in the presence of grid voltage estimation error, Lyapunov's direct method should be employed. For this purpose, a Lyapunov energy function

$$\begin{aligned} \tilde{V}(x) = {} & \tilde{D}(\cos\tilde{\alpha} - \cos(x_1+\tilde{\alpha})) - D(\cos\alpha - \cos(x_1+\alpha)) \\ & + \frac{k_1}{2}x_1^2 + \frac{1}{2}x_2^2, \end{aligned} \tag{20}$$

is proposed in this article. To prove $\tilde{V}(x)$ is a positive definite (PD) function, it should be noted that the terms $\frac{1}{2}x_2^2$ is always PD. Thus, it is enough to assess the rest of the terms in the proposed energy function. To this end, note that the first derivative of $F(x_1) = \tilde{D}(\cos\tilde{\alpha} - \cos(x_1+\tilde{\alpha})) - D(\cos\alpha - \cos(x_1+\alpha)) + \frac{k_1}{2}x_1^2$ with respect to x_1 is

$$\frac{dF(x_1)}{dx_1} = \tilde{D}\sin(x_1+\tilde{\alpha})) - D\sin(x_1+\alpha) + k_1x_1, \tag{21}$$

which is equal to zero at the origin. Also, the second derivative of $F(x_1)$ with respect to x_1 is

$$\frac{d^2F(x_1)}{dx_1^2} = \tilde{D}\cos(x_1+\tilde{\alpha})) - D\cos(x_1+\alpha) + k_1, \tag{22}$$

which is $k_1 - e_1$ at the origin. In order for $\tilde{V}(x)$ to be PD in a neighbourhood W_1, around the origin, $\frac{d^2F(x_1)}{dx_1^2} = k_1 - e_1 > 0, \quad x_1 \in W_1 - \{0\}$, since $F(x_1)$ curvature becomes positive in W_1, making $F(x_1) > 0$ in that neighbourhood excluding the origin. This condition is identical to one of the stability necessary conditions derived from (19).

To find the domain of attraction, the neighbourhood W_2 in which $\dot{\tilde{V}}(x) < 0$ must be found. To this end, consider that

$$\dot{\tilde{V}}(x) = \Big(\tilde{A}\cos(x_1+\tilde{\alpha}) - A\cos(x_1+\alpha) - k_2\Big)x_2^2 \tag{23}$$

is negative definite in a neighbourhood around the origin if $k_2 - e_2 > 0$, which is identical to the second necessary stability condition derived from (19). Ultimately, the equilibrium point domain of attraction can be found as $W = W_1 \bigcap W_2$.

2) Grid Inductance Estimation Error: In this part, the impact of grid inductance estimation error on the system stability is investigated. Based on (8), A, B, C, D, and therefore, α are functions of the grid inductance. Supposing that the system real coefficients are $\tilde{A}$, $\tilde{B}$, $\tilde{C}$, $\tilde{D}$, and $\tilde{\alpha}$, and by applying $\tilde{u}$ to the system, the state-equations can be written as

$$\begin{cases} \dot{x}_1 = x_2, \\ \dot{x}_2 = -\tilde{D}\sin(x_1+\tilde{\alpha}) + D\sin(x_1+\alpha) + \tilde{A}\cos(x_1+\tilde{\alpha})x_2 \\ \quad -A\cos(x_1+\alpha)x_2 + \tilde{B} - B + \tilde{C}x_2 - Cx_2 - k_1x_1 - k_2x_2 \end{cases}. \tag{24}$$

By linearizing the system around the equilibrium point, i.e., the origin, the Jacobian matrix can be found as

$$J = \begin{pmatrix} 0 & 1 \\ -\sqrt{\tilde{D}^2 - \tilde{B}^2} + \sqrt{D^2 - B^2} - k_1 & \tilde{C} - C + \tilde{A}\cos(\tilde{\alpha}) - A\cos(\alpha) - k_2 \end{pmatrix}. \tag{25}$$

By naming

$$\epsilon_1 = -\sqrt{\tilde{D}^2 - \tilde{B}^2} + \sqrt{D^2 - B^2}, \tag{26}$$

and

$$\begin{aligned} \epsilon_2 &= \tilde{A}\cos(\tilde{\alpha}) - A\cos(\alpha) + \tilde{C} - C \\ &= \frac{A}{D}(\sqrt{\tilde{D}^2 - \tilde{B}^2} - \sqrt{D^2 - B^2}) + \tilde{C} - C, \end{aligned} \tag{27}$$

the Jacobian matrix becomes

$$J = \begin{pmatrix} 0 & 1 \\ \epsilon_1 - k_1 & \epsilon_2 - k_2 \end{pmatrix}. \tag{28}$$

Based on (28), the necessary and sufficient conditions for stability are $k_1 > \epsilon_1$ and $k_2 > \epsilon_2$.

C. Design Procedure

As discussed in the previous section, the proposed feedback linearization controller can effectively stabilize an unstable GFLI connected to a weak grid. Additionally, the outer state-feedback controller enables the designer to have any desirable dynamics by placing the closed-loop poles in any arbitrary location. The summary of the design procedure is as follows:

- Choose k_1 and k_2 such that the system has the desirable response. Note that these two variables must be selected such that the current controller dynamics can be neglected, i.e., the PLL is much slower than the current controller.
- Form A, B, C, D, and α by estimating the system states, i.e., x_1 and x_2, as well as the IBR injected power and current. Note that x_2 is the PI controller output, and it is accessible. Also, x_1 is the integral of x_2, which can be approximated by α, i.e., the phase difference between the PoC voltage and the grid. This angle can be estimated based on the injected active power.
- Form the control law, u.
- Integrate the control law and add it to x_2 (the PLL PI controller output or $\Delta\omega$).

IV. Performance Evaluation

To evaluate the performance of the designed feedback linearization controller, the system shown in Fig. 1 with parameters in Table I is implemented in Matlab/Simulink. Furthermore, the performance of the proposed compensator is experimentally assessed using an Imperix inverter, an Imperix B-Box Controller, and a Regatron AC Power Supply. In the simulation tests, the performance of the proposed controller for four different scenarios is evaluated and compared with a conventional PLL: 1) when the GFLI is connected to strong and weak grids, 2) when the estimated grid inductance is not accurate, 3) when a fault occurs at the PoC, and 4) when the grid frequency drops. Additionally, in the experimental tests, it is shown that the system with the proposed controller has a larger domain of attraction than a system equipped with a conventional PLL.

A. Simulation Results

In this part, several simulation tests are conducted on the compensated and conventional systems to evaluate the capabilities of the proposed controller. To this end, the conventional and compensated systems are connected to strong and weak grids, and their performance is contrasted. Additionally, the ability of both systems in dealing with faults while connected to a weak grid is investigated. Finally, the impact of grid inductance estimation error on the compensated system stability is studied. In all of the simulation tests, the control parameters, k_1 and k_2 are set to 1 and 20 for the compensated system making the system damping factor and rise time 0.6 and 150 ms, respectively. Note that the PI controller used in the conventional PLL is $\frac{5s+400}{s}$, which is designed such that the PLL has a high bandwidth and can capture disturbances. It is worth mentioning that the chosen PLL is not necessarily an optimally designed controller for all operating points and SCRs. However, as discussed in the previous section, the proposed compensator forces the whole system to have the desired response regardless of the grid inductance and/or injected power. In the figures shown in provided in this part, unless otherwise stated, (a) shows the three-phase injected currents, (b) is the PoC three-phase voltages, (c) depicts the injected current dq-components, (d) shows $\hat{x}_1$, $\hat{x}_2$, and α, (e) is the injected active and reactive power, and finally, (f) reports the PLL estimated frequency.

TABLE I
The parameters of the study system shown in Fig. 1.

Quantity	Value	Comment
L_{f}	95 μH	Inverter Filter Inductance
R_{f}	0.01 Ω	Series Resistance of L_{f}
L_{g}	250 μH	Grid Inductance
R_{g}	0.025 Ω	Grid Resistance
S_{base}	5 MVA	Inverter Rated Power
SCR	1.15	Grid Short Circuit Ratio (SCR) at S_{base}
v_{g}	690 V	Grid Line-to-Neutral Voltage (rms)
v_{dc}	3000 V	DC Bus Voltage
f_{sw}	5 kHz	PWM Carrier Frequency
f	50 Hz	System Nominal Frequency
K_p	5 $\frac{rad}{V.s}$	PLL controller proportional gain
K_i	400 $\frac{rad}{V.s^2}$	PLL controller integral gain

1) Strong Grid (SCR=17.8): In this part, the grid inductance and resistance are chosen as L_{g}=15 μH and R_{g}=2.5 $m\Omega$, respectively, making SCR=17.8. Also, based on this grid impedance, the PI controller used in the current controller is $1000\times\frac{110\times10^{-6}s+0.0125}{s}$, setting the current controller time constant to 1 ms. Initially, both the conventional and compensated systems inject 2 MW and 0 MVAR to the grid. At t=0.1 s, the active power set-point is changed to 4 MW. Fig. 4 shows the simulation results for the conventional system. It is seen that the conventional system remains stable and tracks its power reference while connected to a strong grid. The simulation results for the compensated system connected to the same grid are shown in Fig. 5. It is seen that the system can inject the requested 4 MW into the grid and remains stable.

Hence, while connected to a strong grid, both conventional and compensated systems remain stable and track their power references. It is worth mentioning that if not perfectly designed, the conventional PLL results in an oscillatory response; however, in the compensated system, the compensator forces the system to have the desired response regardless of the initially designed PLL.

2) Weak Grid (SCR=1.15): In this part, the grid inductance and resistance are chosen as L_{g}=250 μH and R_{g}=25 $m\Omega$, respectively, making SCR=1.15. Also, based on this grid impedance, the PI controller used in the current controller is $1000\times\frac{346\times10^{-6}s+0.035}{s}$, setting the current controller time constant to 1 ms. Similar to the previous tests, both the conventional and compensated systems inject 2 MW and 0 MVAR to the grid, initially. At t=0.1 s, the active power set-point is changed to 4 MW for both systems. Fig. 6 and Fig. 7 show the simulation results for the conventional and compensated systems, respectively. It is observed that both systems initially track their power references. However, after the active power set-point is changed to 4 MW, the conventional system fails to maintain stability, whilst the compensated system remains stable and tracks the power reference with a 150 ms rise time.

3) Grid Impedance Estimation Error: In this scenario, it is assumed that the compensated system is connected to the aforementioned weak grid and injects 2 MW into the grid. In this test, initially, the inductance estimation error is assumed to be zero, i.e., the inductance used in the compensator is accurate. At t=1 s, the grid inductance is jumped to 1.4 times of the initial inductance for 2 s, while the controller remains unchanged. At t=3 s, the grid inductance is reduced to 0.6 of the initial inductance for 2 s. Again, the controller is not changed, and

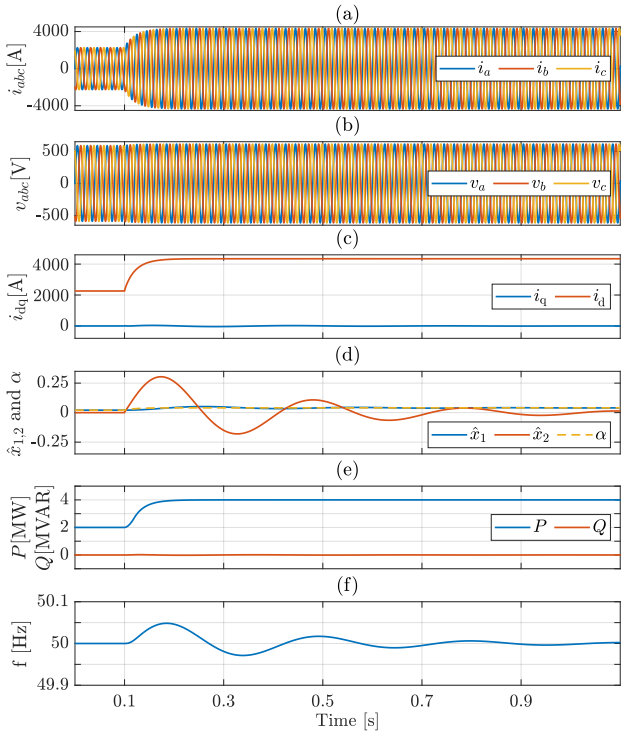

Fig. 4. The simulation results of the conventional system with SCR=17.8 upon active power reference change: a) three-phase grid currents (i_{abc}), b) the PoC three-phase phase voltage c) the dq-components of the grid current (i_{dq}), d) the system states and the power angle, α, e) the injected active and reactive power into the grid, and e) the estimated frequency estimated by the PLL.

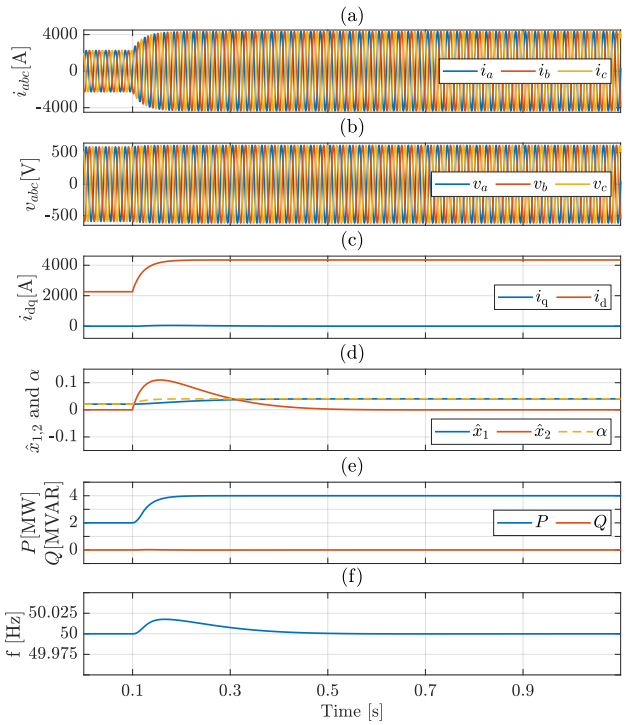

Fig. 5. The simulation results of the compensated system with SCR=17.8 upon active power reference change: a) three-phase grid currents (i_{abc}), b) the PoC three-phase phase voltage c) the dq-components of the grid current (i_{dq}), d) the system states and the power angle, α, e) the injected active and reactive power into the grid, and e) the estimated frequency estimated by the PLL.

the nominal inductance value is used in it. Finally, at t=5 s, the inductance is changed back to the initial inductance the controller is designed for. The simulation results of this scenario are shown in Fig. 8. Fig. 8 (a), (b), (c), and (d) correspond to the injected current dq-components, the states and the power angle, the injected active and reactive power, and the estimated frequency by the PLL, respectively. It is seen that the system can deal with the inductance estimation errors effectively, and the system remains stable while the references are tracked accurately.

4) Grid Frequency Drop: In this scenario, the impact of a grid frequency drop on the compensated system is investigated. In this test, the compensated system is connected to the weak grid with SCR=1.15, and injects 2 MW and 0 MVAR. At t=1 s, the grid frequency drops to 49.5 Hz for one second, and at t=2 s, the frequency returns to 50 Hz. Fig. 9 shows the simulation results of this system. As it is seen, the PLL can capture the frequency before, during, and after the grid frequency step, and the system remains stable at all times.

B. Experimental Results

To experimentally assess the capabilities of the proposed compensator and validate the simulation results, an experimental setup based on Imperix B-Box and Regatron AC power supply is employed as depicted in Fig. 10. The experimental system parameters are presented in Table II. In all experimental tests, the PLL proportional and integral gains are set to 0.1 and 100, respectively. Also, k_1 and k_2 are set to 1 and 20, respectively, for the compensated system throughout the experiments. In the

TABLE II
THE PARAMETERS OF THE EXPERIMENTAL PLATFORM.

Quantity	Value	Comment
L_f	15 mH	Inverter Filter Inductance
R_f	0.5 Ω	Series Resistance of L_f
S_{base}	1 KVA	Inverter Rated Power
v_g	100 V	Grid Line-to-Line Voltage (rms)
v_{dc}	300 V	DC Bus Voltage
f_{sw}	20 kHz	PWM Carrier Frequency
f	50 Hz	System Nominal Frequency

figures depicted in this part, (a) corresponds to the three-phase current, (b) shows the current dq-components, (c) depicts the active and reactive power, and finally, (d) is the PLL estimated frequency.

1) Strong Grid (SCR=30): In the first scenario, both conventional and compensated systems are connected to a strong grid with L_g=1 mH and R_g=30 mΩ, making the SCR=30. Initially, both conventional and compensated systems inject 0.5 kW. At t=0.1 s, the active power reference is changed to 0.8 kW. Fig. 11 and Fig. 12 show the experimental results of this scenario for the conventional and the compensated systems, respectively. As it is observed, the power references are tracked correctly, and the estimated frequency is accurate for both systems.

2) Weak Grid (SCR=2): In this scenario, both conventional and compensated systems are connected to a weak grid with L_g=15 mH and R_g=0.5 Ω, making the SCR=2. Initially, both systems inject 0.5 kW. At t=0.1 s, the active power reference is changed to 0.8 kW. Fig. 13 and Fig. 14 show the experimental results of this scenario for the conventional and the compensated systems, respectively. From the experimental results, it can be

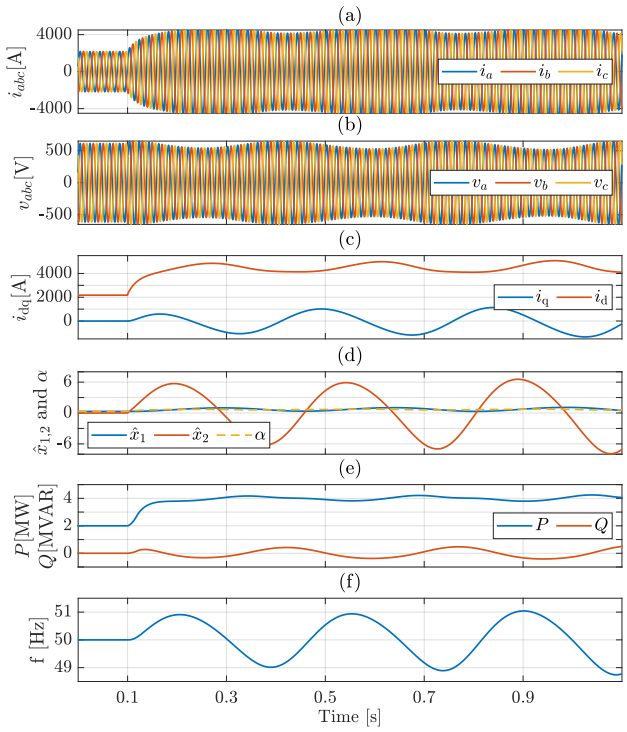

Fig. 6. The simulation results of the conventional system with SCR=1.15 upon active power reference change: a) three-phase grid currents (i_{abc}), b) the PoC three-phase phase voltage c) the dq-components of the grid current (i_{dq}), d) the system states and the power angle, α, e) the injected active and reactive power into the grid, and e) the estimated frequency estimated by the PLL.

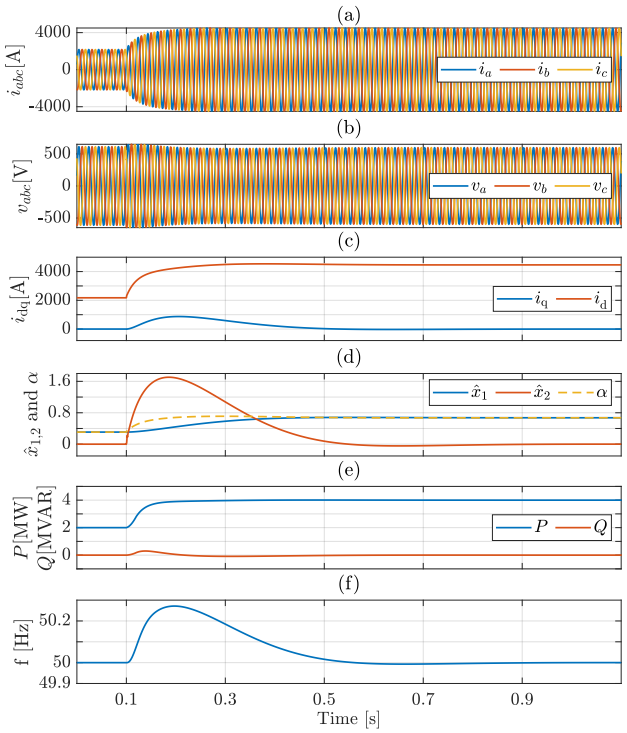

Fig. 7. The simulation results of the compensated system with SCR=1.15 upon active power reference change: a) three-phase grid currents (i_{abc}), b) the PoC three-phase phase voltage c) the dq-components of the grid current (i_{dq}), d) the system states and the power angle, α, e) the injected active and reactive power into the grid, and e) the estimated frequency estimated by the PLL.

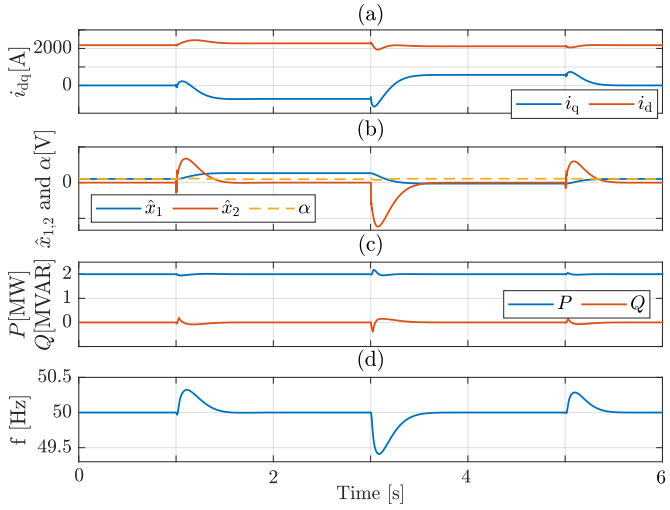

Fig. 8. The simulation results of the compensated system in the presence of grid inductance estimation error: a) the dq-components of the grid current (i_{dq}), b) the system states and the power angle, α, c) the injected active and reactive power into the grid, and d) the estimated frequency estimated by the PLL.

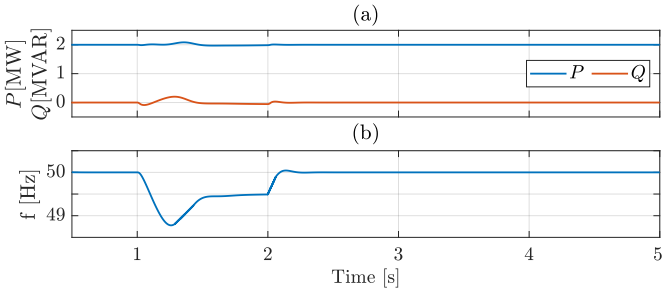

Fig. 9. The simulation results of the compensated system in the presence of grid frequency drop: a) the injected active and reactive power into the grid and b) the frequency estimated by the PLL.

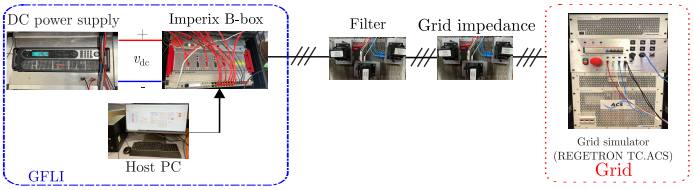

Fig. 10. The experimental setup.

seen that the conventional PLL fails to get synchronized to the grid after the active power reference jumps, and the system becomes unstable; however, the compensated PLL successfully remains synchronized with the grid and retain stability.

3) Stabilizing the Unstable System: In this scenario, initially, the conventional system is connected to the weak grid of the previous test and injects 0.5 kW into the grid. At t=0.1 s, the injected power is increased to 0.8 kW, making the system unstable. After 1.5 s and at t=1.6 s, the compensator is added to the PLL. Fig. 15 shows the experimental results of this scenario. As it is observed, the conventional system is unstable, and oscillations magnitude is increasing. After the feedback linearization compensator is entered to the PLL loop at t=1.6 s, since the equilibrium point domain of attraction is extended, the states are attracted to the equilibrium point, and the initially

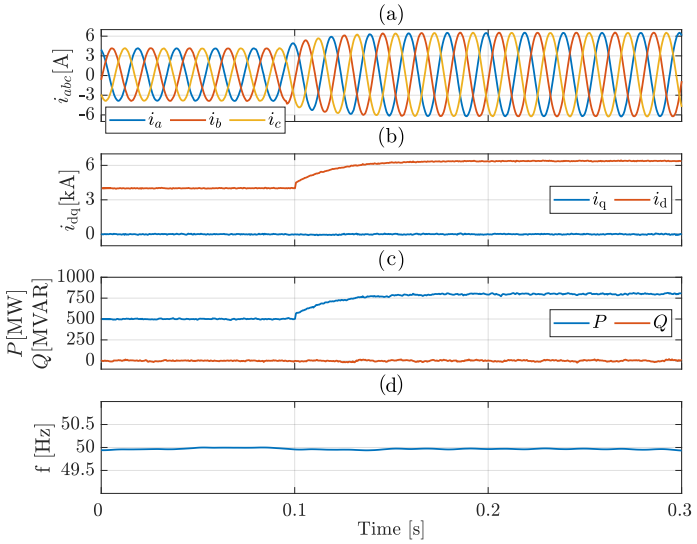

Fig. 11. The experimental results of the conventional system with SCR=30 upon active power reference change: a) three-phase grid currents (i_{abc}), b) the dq-components of the grid current (i_{dq}), c) the injected active and reactive power into the grid, and d) the estimated frequency estimated by the PLL.

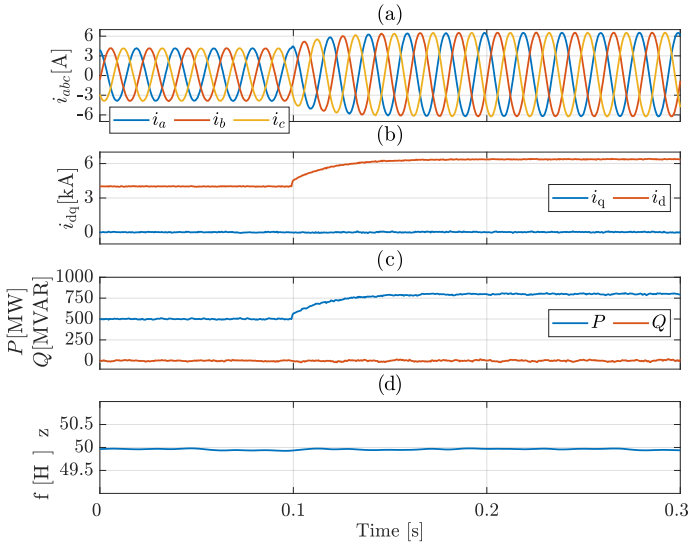

Fig. 12. The experimental results of the compensated system with SCR=30 upon active power reference change: a) three-phase grid currents (i_{abc}), b) the dq-components of the grid current (i_{dq}), c) the injected active and reactive power into the grid, and d) the estimated frequency estimated by the PLL.

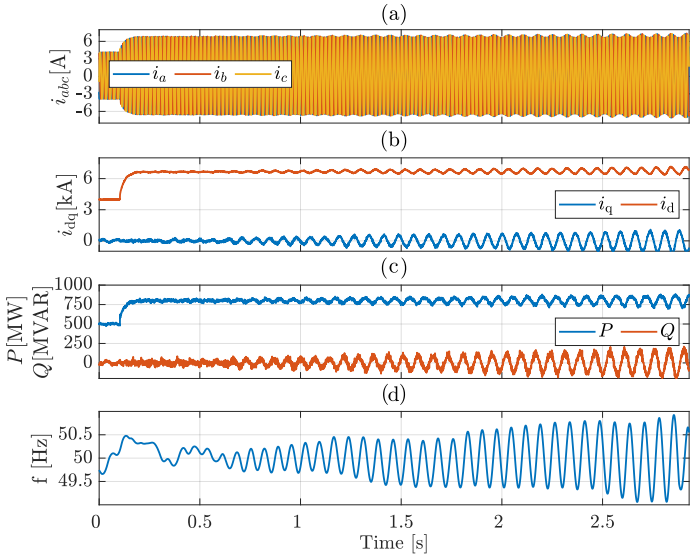

Fig. 13. The experimental results of the conventional system with SCR=2 upon active power reference change: a) three-phase grid currents (i_{abc}), b) the dq-components of the grid current (i_{dq}), c) the injected active and reactive power into the grid, and d) the estimated frequency estimated by the PLL.

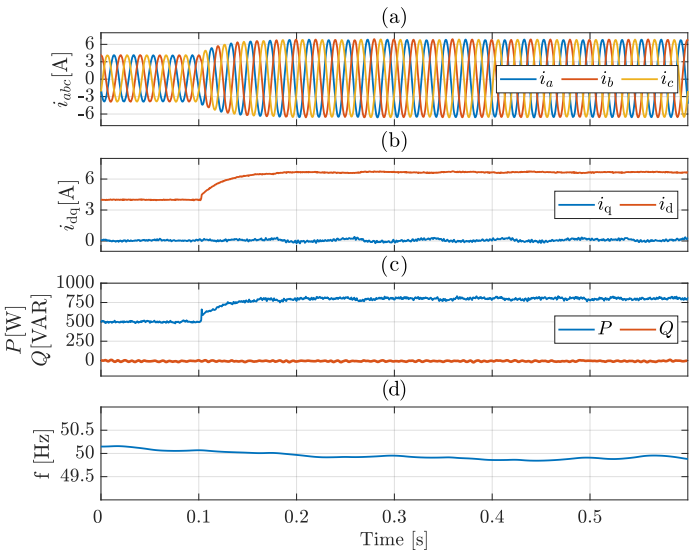

Fig. 14. The experimental results of the compensated system with SCR=2 upon active power reference change: a) three-phase grid currents (i_{abc}), b) the dq-components of the grid current (i_{dq}), c) the injected active and reactive power into the grid, and d) the estimated frequency estimated by the PLL.

unstable system is stabilized.

4) Grid Inductance Estimation Error: In this scenario, the compensated system is connected to a grid with L_g=13 mH and R_g=0.4 Ω. However, the estimated grid inductance used in the compensator is assumed to be 10 mH. Initially, the converter injects 0.5 kW into the grid. At t=0.1 s, the injected power is increased to 0.8 kW. Fig. 16 shows the experimental results of this scenario. As it is observed, the system remains stable under this scenario, despite the error in the grid inductance estimation. This confirms the compensated system is robust against grid impedance estimation discrepancies.

V. Conclusions

This paper proposes a feedback linearization controller that eliminates the nonlinear dynamics of a PLL used in a GFLI. The proposed controller uses the grid impedance and voltage information to expand the domain of attraction to the whole plane to enhance the IBR synchronization in the presence of disturbances, such as operating point changes. Additionally, a state-feedback controller is integrated within the proposed compensator to provide flexibility in the synchronization unit dynamic response, enabling the designer to place the closed-loop system poles at any desirable location. Furthermore, the proposed compensator does not rely on the initially designed PLL performance, which might be degraded due to the changes

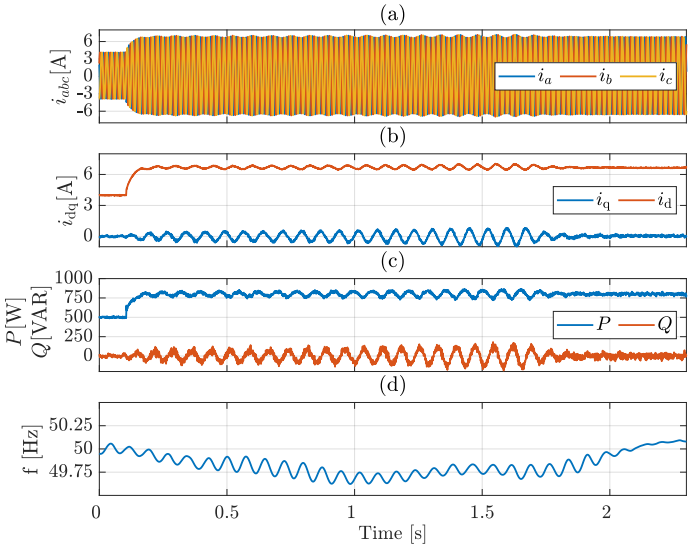

Fig. 15. The experimental results of the system with SCR=2. Initially, a conventional PLL is used in the system. However, after the active power set-point jump that results in instability, the proposed controller is added to the PLL, making the system stable: a) three-phase grid currents (i_{abc}), b) the dq-components of the grid current (i_{dq}), c) the injected active and reactive power into the grid, and d) the estimated frequency estimated by the PLL.

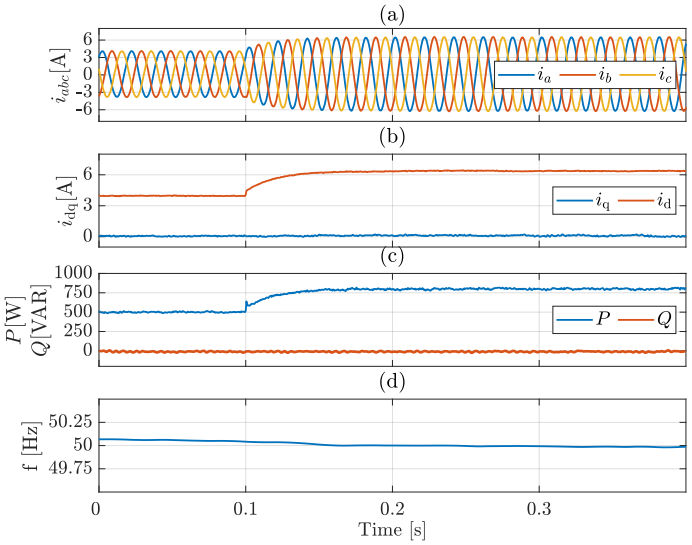

Fig. 16. The experimental results of the system with L_{g}=13 mH, while the impedance used in the compensator is 10 mH: a) three-phase grid currents (i_{abc}), b) the dq-components of the grid current (i_{dq}), c) the injected active and reactive power into the grid, and d) the estimated frequency estimated by the PLL.

in the grid and operating point over time. Besides, it is mathematically shown that the system is robust against discrepancies between the real and estimated system parameters. Finally, the performance and effectiveness of the proposed compensator are validated in various scenarios via simulation and experiment.

REFERENCES

[1] M. G. Taul, X. Wang, P. Davari, and F. Blaabjerg, "An Overview of Assessment Methods for Synchronization Stability of Grid-connected Converters under Severe Symmetrical Grid Faults," *IEEE Transactions on Power Electronics*, vol. 34, no. 10, pp. 9655–9670, 2019.

[2] X. Fu, J. Sun, M. Huang, Z. Tian, H. Yan, H. H.-C. Iu, P. Hu, and X. Zha, "Large-signal stability of grid-forming and grid-following controls in voltage source converter: A comparative study," *IEEE Transactions on Power Electronics*, vol. 36, no. 7, pp. 7832–7840, 2021.

[3] F. Blaabjerg, R. Teodorescu, M. Liserre, and A. V. Timbus, "Overview of control and grid synchronization for distributed power generation systems," *IEEE Transactions on Industrial Electronics*, vol. 53, no. 5, pp. 1398–1409, 2006.

[4] R. H. Lasseter, Z. Chen, and D. Pattabiraman, "Grid-forming inverters: A critical asset for the power grid," *IEEE Journal of Emerging and Selected Topics in Power Electronics*, vol. 8, no. 2, pp. 925–935, 2020.

[5] T. Xia, X. Zhang, G. Tan, and Y. Liu, "All-pass-filter-based PLL for single-phase grid-connected converters under distorted grid conditions," *IEEE Access*, vol. 8, pp. 106 226–106 233, 2020.

[6] A. Luna, J. Rocabert, J. I. Candela, J. R. Hermoso, R. Teodorescu, F. Blaabjerg, and P. Rodríguez, "Grid voltage synchronization for distributed generation systems under grid fault conditions," *IEEE Transactions on Industry Applications*, vol. 51, no. 4, pp. 3414–3425, 2015.

[7] B. Bahrani, S. Kenzelmann, and A. Rufer, "Multivariable-PI-based dq current control of voltage source converters with superior axis decoupling capability," *IEEE Transactions on Industrial Electronics*, vol. 58, no. 7, pp. 3016–3026, 2010.

[8] B. Bahrani, M. Vasiladiotis, and A. Rufer, "High-order vector control of grid-connected voltage-source converters with LCL-filters," *IEEE Transactions on Industrial Electronics*, vol. 61, no. 6, pp. 2767–2775, 2014.

[9] D. B. Rathnayake, M. Akrami, C. Phurailatpam, S. P. Me, S. Hadavi, G. Jayasinghe, S. Zabihi, and B. Bahrani, "Grid forming inverter modeling, control, and applications," *IEEE Access*, 2021.

[10] X. Wang, M. G. Taul, H. Wu, Y. Liao, F. Blaabjerg, and L. Harnefors, "Grid-synchronization stability of converter-based resources—An overview," *IEEE Open Journal of Industry Applications*, vol. 1, pp. 115–134, 2020.

[11] X. Wang and F. Blaabjerg, "Harmonic stability in power electronic-based power systems: Concept, modeling, and analysis," *IEEE Transactions on Smart Grid*, vol. 10, no. 3, pp. 2858–2870, 2019.

[12] D. Yang and X. Wang, "Unified modular state-space modeling of grid-connected voltage-source converters," *IEEE Transactions on Power Electronics*, vol. 35, no. 9, pp. 9702–9717, 2020.

[13] Y. Liao and X. Wang, "Impedance-based stability analysis for interconnected converter systems with open-loop RHP poles," *IEEE Transactions on Power Electronics*, vol. 35, no. 4, pp. 4388–4397, 2019.

[14] M. G. Taul, X. Wang, P. Davari, and F. Blaabjerg, "Current limiting control with enhanced dynamics of grid-forming converters during fault conditions," *IEEE Journal of Emerging and Selected Topics in Power Electronics*, vol. 8, no. 2, pp. 1062–1073, 2019.

[15] ——, "An efficient reduced-order model for studying synchronization stability of grid-following converters during grid faults," in *20th Workshop on Control and Modeling for Power Electronics (COMPEL)*. IEEE, 2019.

[16] H. Wu and X. Wang, "Design-oriented transient stability analysis of pll-synchronized voltage-source converters," *IEEE Transactions on Power Electronics*, vol. 35, no. 4, pp. 3573–3589, 2020.

[17] ——, "Design-oriented transient stability analysis of grid-connected converters with power synchronization control," *IEEE Transactions on Industrial Electronics*, vol. 66, no. 8, pp. 6473–6482, 2019.

[18] J. Rocabert, A. Luna, F. Blaabjerg, and P. Rodriguez, "Control of power converters in ac microgrids," *IEEE Transactions on Power Electronics*, vol. 27, no. 11, pp. 4734–4749, 2012.

[19] M. Z. Mansour, S. P. Me, S. Hadavi, B. Badrazadeh, A. Karimi, and B. Bahrani, "Nonlinear transient stability analysis of phase-locked loop based grid-following voltage source converters using Lyapunov's direct method," *IEEE Journal of Emerging and Selected Topics in Power Electronics*, 2021.

[20] B. Wen, D. Boroyevich, R. Burgos, P. Mattavelli, and Z. Shen, "Analysis of d-q small-signal impedance of grid-tied inverters," *IEEE Transactions on Power Electronics*, vol. 31, no. 1, pp. 675–687, 2016.

[21] K. M. Alawasa, Y. A.-R. I. Mohamed, and W. Xu, "Active mitigation of subsynchronous interactions between pwm voltage-source converters and power networks," *IEEE Transactions on Power Electronics*, vol. 29, no. 1, pp. 121–134, 2014.

[22] J. Fang, X. Li, H. Li, and Y. Tang, "Stability improvement for three-phase grid-connected converters through impedance reshaping in quadrature-axis," *IEEE Transactions on Power Electronics*, vol. 33, no. 10, pp. 8365–8375, 2018.

[23] X. Zhang, D. Xia, Z. Fu, G. Wang, and D. Xu, "An improved feedforward control method considering PLL dynamics to improve weak grid stability of grid-connected inverters," *IEEE Transactions on Industry Applications*, vol. 54, no. 5, pp. 5143–5151, 2018.

[24] M. G. Taul, X. Wang, P. Davari, and F. Blaabjerg, "Systematic approach for transient stability evaluation of grid-tied converters during power system faults," in *IEEE Energy Conversion Congress and Exposition (ECCE)*, 2019, pp. 5191–5198.
[25] H. Geng, L. Liu, and R. Li, "Synchronization and reactive current support of pmsg-based wind farm during severe grid fault," *IEEE Transactions on Sustainable Energy*, vol. 9, no. 4, pp. 1596–1604, 2018.
[26] S. Ma, H. Geng, L. Liu, G. Yang, and B. C. Pal, "Grid-synchronization stability improvement of large scale wind farm during severe grid fault," *IEEE Transactions on Power Systems*, vol. 33, no. 1, pp. 216–226, 2018.
[27] M. G. Taul, X. Wang, P. Davari, and F. Blaabjerg, "Robust fault ride through of converter-based generation during severe faults with phase jumps," *IEEE Transactions on Industry Applications*, vol. 56, no. 1, pp. 570–583, 2020.
[28] B. Weise, "Impact of k-factor and active current reduction during fault-ride-through of generating units connected via voltage-sourced converters on power system stability," *IET Renewable Power Generation*, vol. 9, no. 1, pp. 25–36, 2015.
[29] H. Wu and X. Wang, "Transient stability impact of the phase-locked loop on grid-connected voltage source converters," in *2018 International Power Electronics Conference (IPEC-Niigata 2018 -ECCE Asia)*, 2018, pp. 2673–2680.
[30] ——, "An adaptive phase-locked loop for the transient stability enhancement of grid-connected voltage source converters," in *2018 IEEE Energy Conversion Congress and Exposition (ECCE)*, 2018, pp. 5892–5898.
[31] ——, "Design-oriented transient stability analysis of PLL-synchronized voltage-source converters," *IEEE Transactions on Power Electronics*, vol. 35, no. 4, pp. 3573–3589, 2020.
[32] ——, "Transient angle stability analysis of grid-connected converters with the first-order active power loop," in *2018 IEEE Applied Power Electronics Conference and Exposition (APEC)*, 2018, pp. 3011–3016.
[33] J. H. Suárez, H. M. Gomes, A. J. Sguarezi Filho, D. A. Fernandes, and F. F. Costa, "Grid impedance estimation for grid-tie inverters based on positive sequence estimator and morphological filter," *Electrical Engineering*, 2020.
[34] N. Mohammed, M. Ciobotaru, and G. Town, "Fundamental grid impedance estimation using grid-connected inverters: a comparison of two frequency-based estimation techniques," *IET Power Electronics*, vol. 13, no. 13, pp. 2730–2741, 2020.

Milad Zarif Mansour (S'19) received the B.Sc. degree from the University of Tehran, Tehran, Iran, and the M.Sc. degree from Sharif University of Technology, Tehran, Iran, both in electrical engineering, in 2016 and 2018, respectively. Since 2019, he has been pursuing a Ph.D. degree at Monash University, Melbourne, Australia. His research interests include grid integration of renewable energy resources, control of power electronic devices, and applications of power electronics in power systems.

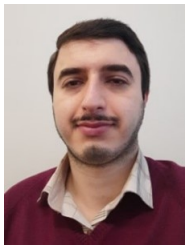

Mohammad Hasan Ravanji Member, IEEE, received his B.Sc., M.Sc. and Ph.D. degrees all in electrical power engineering from Sharif University of Technology (SUT), Tehran, Iran, in 2012, 2014, and 2020, respectively. He was a visiting student with the University of Waterloo, Waterloo, ON, Canada from Oct. 2017 to April 2018. Further, he was with the Iran Grid Management Company (IGMC), Tehran, Iran, as a researcher in their system planning and dynamic studies group from Feb. 2019 to July 2020. He is currently a post-doctoral research fellow at Monash University, Melbourne, Australia. His current research interests include power system stability, renewable energy systems and the application of grid forming and grid following inverters in weak power grids.

Alireza Karimi received the Ph.D. degree in 1997 from Institut National Polytechnique de Grenoble, Grenoble, France. He was an Assistant Professor with the Department of Electrical Engineering, Sharif University of Technology, Tehran, Iran, from 1998 to 2000. Then, he Joined then Ecole Polytechnique Federale de Lausanne (EPFL) in Switzerland and is currently a Professor of automatic control in the Mechanical Engineering Institute of EPFL. Prof. Karimi is the head of "data-driven modelling and control" group in Automatic Control Laboratory and his research interests include data-driven controller design approaches with applications to power grids and mechatronic systems. Prof. Karimi was an Associate Editor of European Journal of Control from 2004 to 2013 and is a member of the conference editorial board of IEEE control systems society since 2018.

Behrooz Bahrani (M'13–SM'19) received the B.Sc. degree from Sharif University of Technology, Tehran, Iran, the M.Sc. degree from the University of Toronto, Toronto, ON, Canada, and the PhD degree from the Ecole Polytechnique Fédérale de Lausanne (EPFL), Lausanne, Switzerland, all in electrical engineering, in 2006, 2008, and 2012, respectively. From September 2012 to September 2015, he was a Postdoctoral Fellow at several institutions including EPFL, Purdue University, West Lafayette, IN, USA, Georgia Institute of Technology, Atlanta, GA, USA, and the Technical University of Munich, Munich, Germany. Since 2015, he has been with Monash University, Clayton, Australia, where currently, he is a Senior Lecturer and the Director of the Grid Innovation Hub. His research interests include control of power electronics systems, applications of power electronics in power and traction systems, and grid integration of renewable energy resources.